Power Losses of Oil-Jet Lubricated Ball Bearings With Limited Applied Load: Part 1-Theoretical Analysis

L. Darul, T. Touret, C. Changenet, Fabrice Ville

Tribology Transactions

ISSN: (Print) (Online) Journal homepage: https://www.tandfonline.com/loi/utrb20

POWER LOSSES OF OIL-JET LUBRICATED BALL BEARINGS WITH LIMITED APPLIED LOAD: PART 1 – THEORETICAL ANALYSIS

L. Darul, T. Touret, C. Changenet & F. Ville

To cite this article: L. Darul, T. Touret, C. Changenet & F. Ville (2023): POWER LOSSES OF OIL-JET LUBRICATED BALL BEARINGS WITH LIMITED APPLIED LOAD: PART 1 – THEORETICAL ANALYSIS, Tribology Transactions, DOI: 10.1080/10402004.2023.2235400

To link to this article: https://doi.org/10.1080/10402004.2023.2235400

Accepted author version posted online: 11 Jul 2023.

POWER LOSSES OF OIL-JET LUBRICATED BALL BEARINGS WITH LIMITED APPLIED LOAD: PART 1 – THEORETICAL ANALYSIS

L. Darul[a,b], T.Touret[a] ,C. Changenet[a,*], F. Ville[b]

[a]Univ Lyon, LabECAM, ECAM LaSalle site de Lyon, 69321 Lyon, France

[b]Univ Lyon, INSA-Lyon, CNRS, LaMCoS, UMR5259,69621 Villeurbanne, France

*christophe.changenet@ecam-lyon.fr; christophe.changenet@ecam.fr

Abstract

This study presents a theoretical analysis to quantify power losses generated by an oil-jet lubricated deep groove ball bearing. Loaded rolling elements (RE) have been thoroughly studied in the past for the Elasto Hydrodynamic Lubricated (EHL) regime, while a well-known problem concerning rolling element bearing (REB) power losses is the estimation of dissipation sources in the case of limited or no applied load. The model presented in this paper aims to solve this problem by describing the physics involved on the unloaded zone. Unloaded RE are considered in an Iso Viscous Rigid (IVR) regime. The model is compared with global power loss models such as Harris-Palmgren or SKF models. This work shows that unloaded RE can generate around 40% of the losses when the applied radial load is about 5% of the static capacity.

KEYWORDS: FRICTION, HYDRODYNAMIC ROLLING, ROLLING ELEMENT BEARING, POWER LOSSES.

INTRODUCTION

The study of power losses in mechanical transmissions is of major interest given the present scientific, economic and environmental challenges. One of the main losses is generated by rolling element bearings (REBs) but the phenomena involved in these rotating components are complex and are still not very well understood. However, there is a consensus about the localization of each power loss in REBs. On Figure 1, the different sources associated with a ball bearing (BB) can be visualized:

1: Losses at outer ring/rolling element contact.

2: Losses at inner ring/rolling element contact.

3: Losses at rings/cage interface.

4: Losses at cage/rolling element interface.

5: Losses at rolling element/fluid interface.

Losses between rings and rolling elements (RE) are composed of two phenomena:

- Sliding over the contact area, occurring because the two surfaces in contact do not have the same speed. This contribution is highly dependent on the applied load.
- Hydrodynamic rolling (HR) at the contact inlet caused by an asymmetrical pressure distribution due to the lubricant flow.

Losses between cage and rings or rolling elements are due to the oil film shearing. Finally, the losses between rolling elements and fluid are also composed of two phenomena:

i) Drag losses: rolling elements are moving through a mixture of air and oil. This motion generates a drag force.

ii) Churning losses: rolling elements are also spinning in the same fluid which contributes to shear it.

Those phenomena can be modelled by two main approaches that can be found in the literature. Firstly, a local approach can be mentioned which aims to predict REB power losses by calculating each local contribution inside the bearing:

- Contribution associated with sliding is studied for a long time [2-5].
- Hydrodynamic rolling generates a resistive torque on the REB. It has been first studied by Tevaarwerk [6] who considers this force as the resultant of pressure along the contact. Other authors [7-9] studied this force as a resultant of traction and sliding effects.
- Oil shearing between cage and rolling elements, or between cage and rings, are generally modelled as a journal bearing [10-11] and are generally negligible [10].
- As far as churning and drag phenomena are concerned, several studies have been done to analyze this contribution at high rotational speeds [10-14]. These losses dominate the others when the product N·dm is greater than 10^6[10]. However, for low to moderate speeds, this contribution is limited.

The local models found in the literature (e.g. in [15-17]) do not consider all the contributions in the same way. In general, it is found that the prediction of power losses is better when the HR is considered [15,16]. This contribution is commonly calculated on the loaded zone and is considered as load dependent. However, the behavior of the unloaded zone is rarely investigated.

The second approach is the global one. The idea is to predict the REB power losses without knowing specifically each contribution and without accurate information on internal geometry and kinematics. In this field, two global models are generally found:

- Harris and Palmgren model [18,19], which is based on experimental testing. The loss torque is divided into load-independent and load-dependent contributions. A good agreement is found between experimental results and this model even if parameters, such as f_0 and f_1, need to be recalibrated from experiments [20-21].
- SKF model [22] which gives analytical relationships to estimate the total loss torque divided into a rolling frictional torque, a sliding one, drag losses and seal losses. A good agreement is also found between this model and experiments. However, correction factors derived from experiments are also necessary [23-24].

For low to moderate speeds (n·dm product lower than 10^6) without applied load, experiments show that there are power losses [25]. This matter is well predicted by Harris model which does not consider the drag contribution. This brings up a question: which contribution is responsible for the load independent power losses?

To investigate this question, the authors propose to use Houpert's work on hydrodynamic loading in REB [26]. This approach is used in a complete local model and compared with global models. In the present study, deep groove ball bearings are considered, the range of considered speeds is low to moderate (as for Palmgren's experiments, with N·dm lower than 10^6). Only a low radial load is applied (about 5 to 10% of the REB static capacity) and the REBs are oil-jet lubricated.

The study performed by the authors is divided in two parts. This paper corresponds to the first one which aims to propose a new power loss model. A companion paper [27], which corresponds to a second part, focuses on experimental validations.

The proposed model is a local one. Drag contribution is neglected as the rotational speed range is considered as moderate. Only sliding and hydrodynamic rolling are considered and the description of the contacts in the REB is therefore necessary. Thus, first part of the paper concerns the implementation of a quasi-static model. The next part describes the power loss calculations. Then, the two main global models found in the literature are described and a numerical comparison is carried out between the existing models and the proposed one.

QUASI-STATIC MODEL

In order to evaluate the power losses at each contact in the REB, a quasi-static model based on Jones analysis [2], well detailed in [19], is implemented. This section summarizes the main steps.

REB Geometry

The macro geometry (external and internal diameters, …) of the REB is considered as known. However, other parameters need to be evaluated:

a) The free contact angle (when no load is applied) α^0 (Figure 2 (a)) is defined as:

$$\alpha^0 = cos^{-1}\left(1 - \frac{P_d}{2A}\right) \qquad (1)$$

Where P_d is the diametral clearance of the REB and A is the distance between raceway groove curvature centers (r_o, r_i), defined as:

$$A = r_o + r_i - D \qquad (2)$$

b) The geometrical ratio γ:

$$\gamma = \frac{cos\ \alpha \cdot D}{d_m} \qquad (3)$$

Where α is the contact angle, D the ball diameter and d_m the mean diameter.

c) The equivalent radii in the rolling direction ($\vec{x}$) and transverse one ($\overrightarrow{y}$) are defined for inner and outer rings as:

$$\begin{cases} Rx_i = \dfrac{D(1-\gamma)}{2} \\ Rx_o = \dfrac{D(1+\gamma)}{2} \end{cases} \qquad (4) \qquad \begin{cases} Ry_i = \dfrac{f_i\, D}{2f_i - 1} \\ Ry_o = \dfrac{f_o\, D}{2f_o - 1} \end{cases} \qquad (5)$$

Distribution of internal loading

The objective is to calculate the load applied on each ball, located at a position ψ (Figure 2 (b)). In the present study, the rotational speed range is considered as moderate. Both centrifugal force and gyroscopic moment are not considered leading to similar contact angles and loads on inner and outer rings. Moreover, only radial load is applied, so axial deformation and contact angles are equal to zero. From this hypothesis, REB global equilibrium can be written as:

$$F_r = \sum_{j=1}^{j=Z} Q_{n_j} \cos\psi_j \qquad (6)$$

and the load Q_{n_j} is related to the REB radial displacement δ_r:

$$Q_{n_j} = K_n \left(\delta_r \cos\psi_j - \frac{1}{2} P_d \right)^{1.5} \qquad (7)$$

where K_n is a load-deflection factor defined in [19].

Finally, the global equilibrium is reached for an optimal value δ_r.

LOCAL POWER LOSS MODEL

Sliding and hydrodynamic rolling are localized power loss phenomena on the contact area which is an ellipse for ball bearings. From the estimation of the load distribution, the dimensions of this area can be calculated.

Ball/Ring Contact Area

a is the ellipse dimension in the transverse rolling direction ($\vec{y}$):

$$a_j = a' \cdot \left(\frac{3\pi \cdot Q_{n_j}}{2 \cdot \rho_{equiv} \cdot E'} \right)^{1/3} \qquad (8)$$

and b the ellipse dimension in the rolling direction ($\vec{x}$):

$$b_j = b' \cdot \left(\frac{3\pi \cdot Q_{n_j}}{2 \cdot \rho_{equiv} \cdot E'} \right)^{1/3} \qquad (9)$$

with E' the equivalent Young modulus; ρ_{equiv} the curvature sum; a' and b' the ellipse dimensionless parameters, given in [19].

Sliding

Assuming a constant friction coefficient μ_{sl}, the sliding force on each contact can be

$$F_{sl_j} = \mu_{sl}\, Q_{n_j} \qquad (10)$$

estimated from [28] as:

As a first approximation, μ_{sl} is assumed to be 0.05, consistent with global models [22].

The sliding velocity v_{sl} can be estimated from Jones [2] and Harris analysis [19]. Finally,

$$P_{sl} = \mu_{sl} \sum_{1}^{j=Z} Q_{n_j} \left(v_{sl_{o_j}} + v_{sl_{i_j}} \right) \qquad (11)$$

power losses from sliding on inner and outer rings are:

Hydrodynamic Rolling EHL Regime

Hydrodynamic rolling is due to an asymmetric pressure distribution. In REBs, classical calculations use EHL theory to quantify power losses due to hydrodynamic rolling. This contribution can be calculated using Tevaarwerk [6] formula:

$$F_{HR_{EHD}} = Q_{n_j} \frac{a}{R_x} \left[4{,}25\, G^{*0{,}022}\, W^{*-0{,}87}\, U^{*0.66} \left(\frac{b}{a}\right)^{0.91} \right] \quad (12)$$

With, U*, G*, W*, the well-known dimensionless parameters:

$$U^* = \frac{v_r\, \eta}{E'\, R_x}\ ;\ G^* = \alpha_p E'\ ;\ W^* = \frac{Q_{n_j}}{E'\, R_x^2} \quad (13)$$

Rolling velocity v_r is calculated as the average point of contact velocity of both the ring and the rolling element:

$$v_r = \frac{1}{2}\left(\frac{D}{2}\omega_R + \left(\frac{d_m}{2} - \frac{D}{2}\right)(\omega - \omega_c)\right) \quad (14)$$

The ball rotation speed ω_R and the cage rotational speed ω_c are defined in [19].

Hydrodynamic Rolling IVR Regime

The EHL regime is observed when applied load and speed are sufficiently high, which is highlighted by Moes' parameters [29]: L and N. Therefore, loaded rolling elements (RE) are without any doubt in EHL regime. Nevertheless, in all previous studies, the influence of unloaded RE on power losses has always been neglected. As no load is applied on these REs, lubrication regime is no longer EHL but Iso Viscous Rigid (IVR). Then hydrodynamic loading on unloaded REs due to IVR regime can be added.

From [9], hydrodynamic rolling force in IVR can be calculated as:

$$F_{HR_{IVR}} = 0.835\ (\lambda)^{-0.358} W^{*0{,}364} (2U^*)^{0.636}\ E'\ R_x^2 \quad (15)$$

With $\lambda = \frac{R_x}{R_y}$

The hydrodynamic rolling force still depends on the load. The authors propose a new approach to overcome this issue. An equivalent load is calculated from the film thickness. Film thickness in IVR regime can be expressed from [30]:

$$h_{0_{IVR}} = 128\, R_x \left(\frac{U^*}{W^*}\right)^2 \frac{1}{\left(1+\frac{2\lambda}{3}\right)^2 \lambda} \left(0.13 \operatorname{atan}\frac{1}{2\lambda} + 1.68\right)^2 \quad (16)$$

It can be seen in equation (16) that, for W^* equals 0 (unloaded RE), film thickness tends to infinity. Of course, this cannot occur in REBs. The basic assumption made by authors is that the film thickness is set to the space between RE and rings. Thus, the film thickness is set to $\frac{Pd}{4}$ in equation (16). From this assumption, an equivalent load can be calculated:

$$Q_{eq} = E'\, R_x^2 \left[128\, R_x\, \frac{U^{*2}}{\frac{P_d}{4}} \frac{1}{\left(1+\frac{2\lambda}{3}\right)^2 \lambda} \left(0.13\ \operatorname{atan}\frac{1}{2\lambda} + 1.68\right)^2\right]^{\frac{1}{2}} \quad (17)$$

This equivalent load can then be used to estimate hydrodynamic rolling force in the REB based on Equation (15).

From a physical point of view, even when no load is applied, some power losses are still generated since power losses in IVR are only related to REB geometry, speed and lubricant properties.

Finally, power losses from hydrodynamic rolling are calculated with:

$$P_{HR} = F_{HR}\, v_r \quad (18)$$

With $F_{HR} = F_{HR_{EHD}}$ for loaded ER and $F_{HR} = F_{HR_{IVR}}$ for unloaded ER.

GLOBAL POWER LOSS MODELS

The results obtained from the proposed model can be compared to those estimated from well-known power loss models briefly summarized below: Harris-Palmgren [18,19] and SKF [22].

Harris-Palmgren

This model is built from experiments and is composed of two contributions:

- Load-dependent one:

$$M_1 = f_1 \, F \, d_m \tag{19}$$

- Independent of load one:

$$M_0 = f_0 \, 10^{-10} \, d_m^3 \, (\nu N)^{2/3} \tag{20}$$

The power losses of each contribution are added:

$$P_{Harris} = \frac{(M_0 + M_1)}{1000} \, N \, \frac{\pi}{30} \tag{21}$$

f_0 parameter varies between 1 and 4 for deep groove ball bearings depending on the lubrification. For oil-jet lubrication, f_0 should be 4 even if previous studies have shown that this value may be too high [20].

Harris-Palmgren model has been elaborated in the 1950's and the operating conditions of the tests are not well known. It is difficult to establish the validity of the model for any speed, temperature, load, ... However, this model is very useful because only a few pieces of information are needed to estimate power losses: the applied load, the mean diameter, the ring temperatures, and the rotational speed. The main inconvenient is that the f_0 parameter needs to be experimentally recalibrated for each REB.

SKF

It is composed of three physical contributions (seals are not considered here):

- Hydrodynamic rolling

$$M_{rr} = \phi_{rs}\, \phi_{ish}\, G_{rr}\, (\nu N)^{0,6} \tag{22}$$

With: ϕ_{rs} a replenishment factor and ϕ_{ish} a thermal reduction factor, highly dependent on viscosity and speed, and for a deep groove ball bearing:

$$G_{rr} = R_1\, d_m^{1.96}\, F_r^{0.54} \tag{23}$$

- Sliding

$$M_{sliding} = G_{sl}\, \mu_{sl} \tag{24}$$

With for a deep groove ball bearing:

$$G_{sl} = S_1\, d_m^{-0.26}\, F_r^{\frac{5}{3}} \tag{25}$$

And $\mu_{sl} = 0.05$ for lubrication with mineral oil. Values for other lubricants can be found in [22].

- Drag

$$M_{drag} = 0.4\, V_M\, K_{bille}\, d_m^5\, N^2 + 1{,}093\, 10^{-7}\, N^2\, d_m^3 \left(\frac{N\, d_m^2\, f_t}{\nu}\right)^{-1,379} R_s \tag{26}$$

Finally, power losses from these contributions equal:

$$P_{SKF} = \frac{\left(M_{rr} + M_{sl} + M_{drag}\right)}{1000}\, N\, \frac{\pi}{30} \tag{27}$$

All the parameters are fully explained in [22], they depend on REB geometry, lubrication, and speed.

On one hand, Niel [20] showed that good correlation can be found between SKF model and experiment for high temperatures and low load by modifying SKF model. The applied load is limited to 10% of C0. A thermal network is used instead of ϕ_{ish} factor and drag contribution is not considered. On the other hand, Fernandes [24] showed that SKF model is suitable for low speeds and high loads.

COMPARISON OF THE MODELS

The results are calculated for a 6210Z deep groove ball bearing, oil jet lubricated. Oil, REB, and steel characteristics are given in Table 1, Table 2, and Table 3. Oil viscosity is calculated with mathematical relationship given in [31]:

Evolution with Speed and Temperature

A set of simulations is performed to compare the behavior of the models with different speeds and lubricant temperatures. The considered load is 1kN (5% of the static capacity). The load distribution is shown on Figure 3. It can be seen that a limited number of balls are loaded. Viscosity is calculated for two temperatures: 30°C (a) and 90°C (b). As previously mentioned, f_0 parameter used in Harris model must be evaluated experimentally. Nevertheless, with this type of REB and these lubrication conditions, the value of this parameter is generally between 1 and 2[14,21]. Therefore, Harris model is calculated and plotted for these two values. f_1 value taken is the one given by Harris [19]: $f_1 = 0.005 * \left(\frac{F_r}{C_0}\right)^{0.55}$. Figure 4 shows the comparison between the different models as a function of the inner ring rotational speed.

For moderate speeds (up to around 10 000rpm - i.e., equivalent n·dm product is 700 000), the evolution of power losses is similar for the different models. Power losses are multiplied by 3 when speed is doubled. This behavior is consistent with the $\frac{2}{3}$ power on the contribution of

speed on resistive torque. However, SKF model has a divergent behavior for higher speeds (above 10 000 rpm).

As far as temperature dependencies are concerned, when comparing at low and high temperatures, the power losses are reduced by only 15% for the SKF model. In comparison, Harris and the proposed model have a significant temperature dependency (losses have been reduced by 3 for Harris model and 4 for the proposed model). This highlights that temperature and so viscosity, is considered differently in the different models.

Figure 5 shows the power loss contributions for two speeds (3200rpm and 9800 rpm) and two temperatures (30°C and 90°C). Firstly, for the considered operating conditions, Harris model is largely composed of the load-independent contribution (at 3200rpm, around 92% at high temperature and 80% at low temperature). This contribution becomes even more important at higher speed.

For SKF model, hydrodynamic rolling (HR) and drag are the main sources of dissipation. Indeed, sliding is very low because of the low considered load. The distribution between drag and HR is slightly dependent on the temperature (at 3200 rpm, HR represents 69% of power losses at low temperature and 58% for higher temperatures). However, the distribution is much more dependent on speed (at 30°C, HR represents 69% of power losses at 3200 rpm and 29% at 9800 rpm). Since for SKF model the drag contribution is the majority and varies little with temperature, the global power loss depends little on temperature.

In the proposed model, power losses associated to sliding are very low, which is consistent with SKF model. Contribution of HR in EHL regime is almost the same in comparison with SKF model. The major difference comes from the power losses added by the unloaded RE in IVR regime. At 3200 rpm and at low temperature, this contribution represents 52% of the power losses and 35% at high temperature. Moreover, this contribution becomes more

important at high speed: at 9800 rpm, it represents 62% of the power losses at low temperature and 42% at high temperature. Thus, by not considering this contribution, almost half of the power losses are neglected in the REB. Existing local power loss models only consider sliding and HR in EHL regime on loaded RE. Hence, as it can be seen in Figure 5, power losses calculated with these two contributions cannot match the minimum values calculated by global models.

Evolution with Load

A new set of simulations is performed (at 3200 rpm and 30°C) to compare the behavior of the models with various loads. In Figure 6, the variation of load is studied for each model. It can be noticed that the slope is similar for SKF and the proposed model. This is due to the HR in EHL regime: load varies to the power 0.5 in both models. For low loads:

i) SKF model estimated power losses are low and much lower compared to the other models. It is due to sliding and rolling which represent a small contribution.

ii) In Harris model, the load independent contribution (M0) is still important.

iii) The proposed model predicts power losses thank to HR in IVR regime. Furthermore, the power losses calculated with the proposed model are always in between the values given by Harris model for the two limits of f_0 (1 and 2). Considering only sliding and HR in EHL regime on loaded RE, calculated power losses are zero when no load is applied.

CONCLUSION

A new power loss model for oil-jet lubricated deep groove ball bearing is presented. This model is based on a quasi-static approach that provides accurate information about the contact areas. Then, sliding and hydrodynamic rolling (in EHL regime on loaded RE and in IVR regime on unloaded RE) are calculated for each contact. The proposed model was compared

to the two main power loss models found in literature: Harris-Palmgren and SKF. The evolution of the different models with respect to speed is similar. However, there is a notable difference in behavior with temperature. This is mainly due to drag contribution in SKF model which is almost temperature independent.

At low load, the proposed model still gives power losses equivalent to Harris model due to hydrodynamic rolling contribution on the unloaded rolling elements. Finally, the new model does not require experimental recalibration, the only information needed are the REB geometry, oil properties and the operating conditions, unlike the Harris model.

A complementary paper deals with the experimental validation of the model as the different models do not give the same results.

NOMENCLATURE

a	Semi-major axis of the elliptical contact area, m
b	Semi-minor axis of the elliptical contact area, m
A	Distance between raceway groove curvature centers, m
d_m	Mean diameter, m
D	Rolling element diameter, m
E'	Equivalent Young modulus = $\frac{2}{\left[\frac{1-\nu_1^2}{E_1}+\frac{1-\nu_2^2}{E_2}\right]}$, Pa
f	Osculation = r/D , -
f_0, f_1	Harris parameters, -
F_{HR}	Hydrodynamic rolling force, N
F_r	Radial load, N
F_{sl}	Sliding force, N
G^*	Dimensionless materials parameter = $\alpha\ E'$, -
h_0	Film thickness, m
K	Load-deflection factor, $N.mm^{-1.5}$
M	Loss torque of the global models, $N.mm$
N	Rotational speed, rpm
P_d	Diametral clearance, m
P	Power losses, W

Q_n	Load on a ball, N
r	Raceway groove curvature radius, m
R_x, R_y	Equivalent radii, m
U^*	Dimensionless speed = $\frac{v_r \eta}{E' R_x}$, -
v_r	Rolling velocity, $m.s^{-1}$
v_{sl}	Sliding velocity, $m.s^{-1}$
W^*	Dimensionless load = $\frac{Q}{E' R_x^2}$, -
Z	Number of rolling elements, -
α^0	Free contact angle, rad
α	Contact angle, rad
α_p	Pressure-viscosity coefficient, Pa^{-1}
γ	Geometrical ratio, -
λ	Radii ratio = R_x/R_y,-
ρ_{equiv}	Curvature sum, m^{-1}
δ	Deflection or contact deformation, m
η	Dynamic viscosity, $Pa.s$
ν	Kinematic viscosity, $mm^2.s^{-1}$ (cSt)
μ_{sl}	Friction coefficient, -

ψ	Location angle of a ball, rad
ω	Rotational speed, $\mathrm{rad.\,s^{-1}}$
i	Refers to inner ring
o	Refers to outer ring
j	Refers to ball number

REFERENCES

[1] Niel, D. (2019), “Etude Du Comportement Thermomécanique de Paliers à Roulements Pour Une Application Hautes Vitesses,” Doctoral Thesis, INSA Lyon, Université de Lyon.

[2] Jones, A. B. (1959), “Ball Motion and Sliding Friction in Ball Bearings,” ASME. Journal of Basic Engineering, **81**(1), pp 1–12.

[3] Heathcote, H. L. (1920), “The ball bearing: in the making, under test and on service,” Proceedings of the Institution of Automobile Engineers, **15**(1), pp 569–702.

[4] Poritsky, H., Hewlett, C. W., Jr. and Coleman, R. E. (1947) "Sliding Friction of Ball Bearings of the Pivot Type," ASME. Journal of applied Mechanics, **14**(4), pp 261-268.

[5] Johnson, K. L. (1959), "The Influence of Elastic Deformation Upon the Motion of a Ball Rolling Between Two Surfaces," Proceedings of the Institution of Mechanical Engineers, **173**(34), pp 795-810.

[6] Tevaarwerk, J. L., and Johnson, K. L. (1979), "The Influence of Fluid Rheology on the Performance of Traction Drives," ASME. Journal of Technology, **101**(3), pp 266–273.

[7] Houpert, L. (1987), “Piezoviscous-Rigid Rolling and Sliding Traction Forces, Application: The Rolling Element–Cage Pocket Contact,” ASME. Journal of Tribology, **109**(2), pp 363–370.

[8] Zhou, R. S., and Hoeprich, M. R. (1991), “Torque of Tapered Roller Bearings.,” ASME. Journal of Tribology, **113**(3), pp 590–597.

[9] Biboulet, N., and Houpert, L. (2010), “Hydrodynamic Force and Moment in Pure Rolling Lubricated Contacts. Part 2: Point Contacts,” Proceedings of the Institution of Mechanical Engineers, Part J: Journal of Engineering Tribology, **224**(8), pp. 777–787.

[10] Pouly, F., Changenet, C., Ville, F., Velex, P., and Damiens, B. (2010), “Power Loss Predictions in High-Speed Rolling Element Bearings Using Thermal Networks,” Tribology Transactions, **53(**6), pp 957-967.

[11] Nelias, D., Sainsot, P., and Flamand, L. (1994), “Power Loss of Gearbox Ball Bearing Under Axial and Radial Loads,” Tribology Transactions, **37**(1), pp 83-90.

[12] Parker, R., J. (1984), "Comparison of predicted and experimental thermal performance of angular contact ball bearings," Nasa Technical Paper, **2275**, pp 1-20.

[13] Marchesse, Y., Changenet, C., Ville, F., and Velex, P. (2014), “Numerical Investigations on Drag Coefficient of Balls in Rolling Element bearings,” Tribology Transactions, **57**(5), pp 778-785.

[14] Niel, D., Changenet, C., Ville, F., and Octrue, M. (2019), “Thermomecanical Study of High Speed Rolling Element Bearing: A Simplified Approach,” Proceedings of the Institution of Mechanical Engineers, Part J: Journal of Engineering Tribology, **233**(4), pp 541–552.

[15] Zhao, Y., Zi, Y., Chen, Z., Zhang, M., Zhu, Y., Yin, J. (2023), “Power loss investigation of ball bearings considering rolling-sliding contacts,” International Journal of Mechanical Sciences, **250**, 108318.

[16] Kerrouche, R., Dadouche, A., Mamou, M., Boukraa, S. (2021), “Power Loss Estimation and Thermal Analysis of an Aero-Engine Cylindrical Roller Bearing,” Tribology Transactions, **64**(6), pp 1079-1094.

[17] Zhou, S., Singh, A., Kahraman, A., Hong, I. et al. (2023), "Power Loss Studies for Rolling Element Bearings Subject to Combined Radial and Axial Loading," SAE Technical Paper 2023-01-0461.

[18] Palmgren, A. (1967), “Les roulements : description, théorie, applications” Second edition, SKF Group, 241 p.

[19] Harris, T. A. (1991), “Rolling Bearing Analysis,” Third Edition, John Wiley and Sons Inc., New York, USA, ISBN 0 471 51349 0.

[20] Niel, D., Changenet, C., Ville, F., and Octrue, M. (2018), “A New Test Rig to Study Rolling Element Bearing Thermomechanical Behavior,” International Gear Conference, Lyon, pp 121–133.

[21] Brossier, P., Niel, D., Changenet, C., Ville, F., and Belmonte, J. (2021), “Experimental and Numerical Investigations on Rolling Element Bearing Thermal Behaviour,” Proceedings of the Institution of Mechanical Engineers, Part J: Journal of Engineering Tribology, **235**(4), pp 842–853.

[22] SKF Group (2013), “Rolling bearings”, SKF Group, 1375 p.

[23] Cousseau, T., Graça, B., Campos, A., and Seabra, J. (2011), “Friction Torque in Grease Lubricated Thrust Ball Bearings,” Tribology International, **44**(5), pp 523–531.

[24] Fernandes, C. M. C. G., Martins, R. C., and Seabra, J. H. O. (2013), “Friction Torque of Thrust Ball Bearings Lubricated with Wind Turbine Gear Oils,” Tribology International, **58**, pp 47–54.

[25] Yilmaz, M., Lohner, T., Michaelis, K., Stahl, K. (2020), “Bearing Power Losses with Water-Containing Gear Fluids,” Lubricants, **8**(5), pp 1-11.

[26] Houpert, L. (2016), “Hydrodynamic Load Calculation in Rolling Element Bearings,” Tribology Transactions, **59**(3), pp 538-559.

[27] de Cadier de Veauce, F., Darul, L., Marchesse, Y., Touret, T. , Changenet, C., Ville, F., Amar, L. and Fossier,C. (2023), "Power Losses of Oil-Jet Lubricated Ball Bearings With Limited Applied Load: Part 2 - Experiments and Model Validation," Tribology Transactions.

[28] Coulomb, C. A. (1821), “Théorie Des Machines Simples,” Bachelier, 387 p.

[29] Moes, H. (1992), “Optimum similarity analysis with applications to elastohydrodynamic lubrication,” Wear, **59**(1), pp 57-66.

[30] Brewe, D. E., and Hamrock, B. J. (1982), "Analysis of Starvation Effects on Hydrodynamic Lubrication in Nonconforming Contacts," ASME. Journal of Lubrication Technology, **104**(3), pp 410–417.

[31] ASTM D 341-93 (1998), “Standard viscosity–temperature charts for liquid petroleum products,” ASTM International.

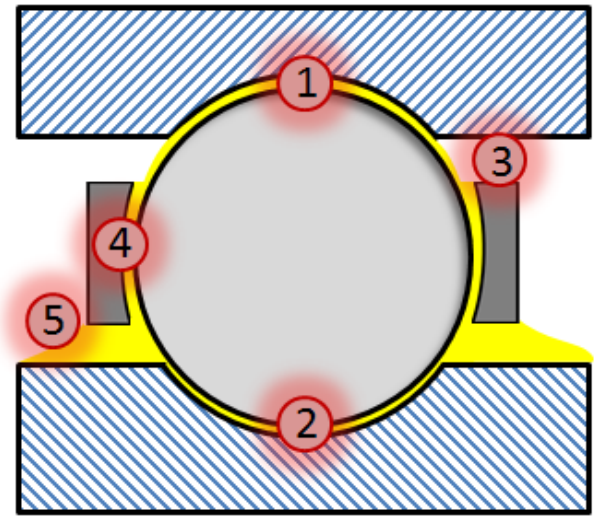

Figure 1 Power loss sources in a ball bearing [1]

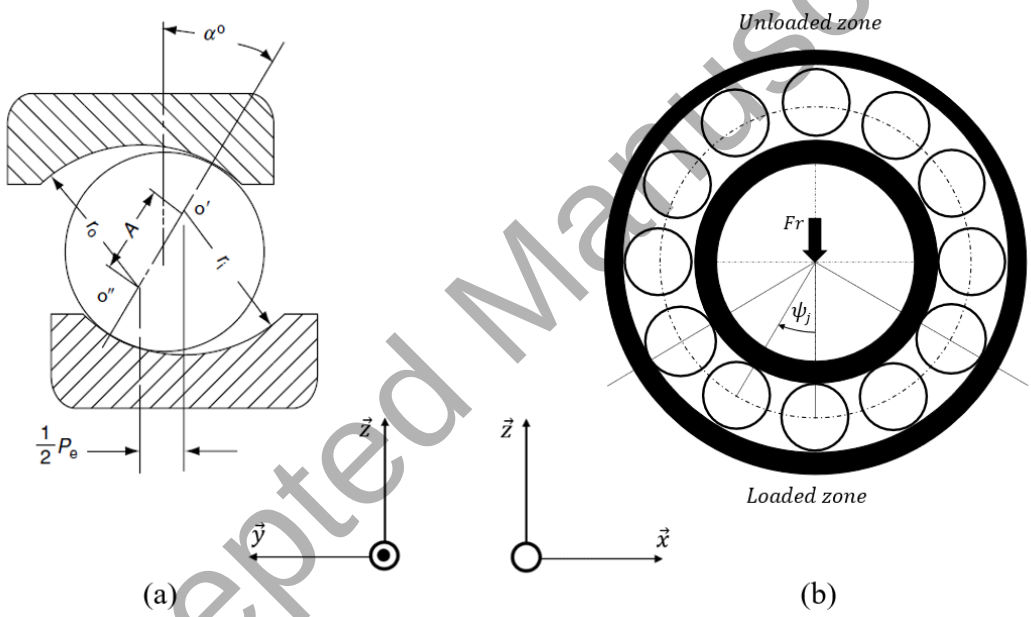

Figure 2 (a) Free contact angle [19] (b) Ball location and the loaded zones

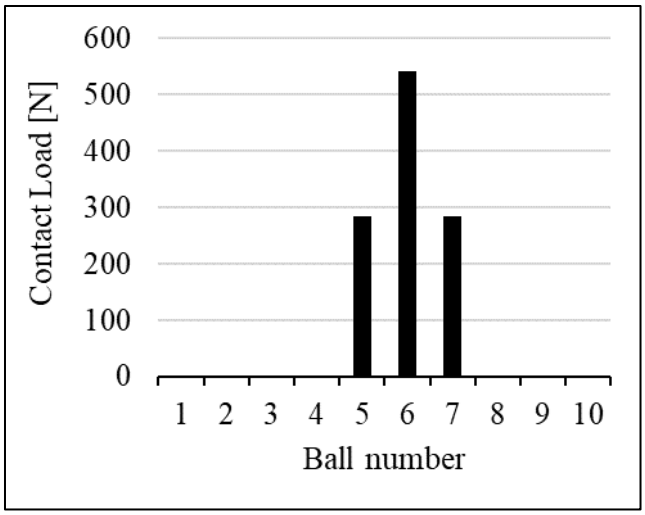

Figure 3 Load distribution on 6210Z REB – Fr = 1kN

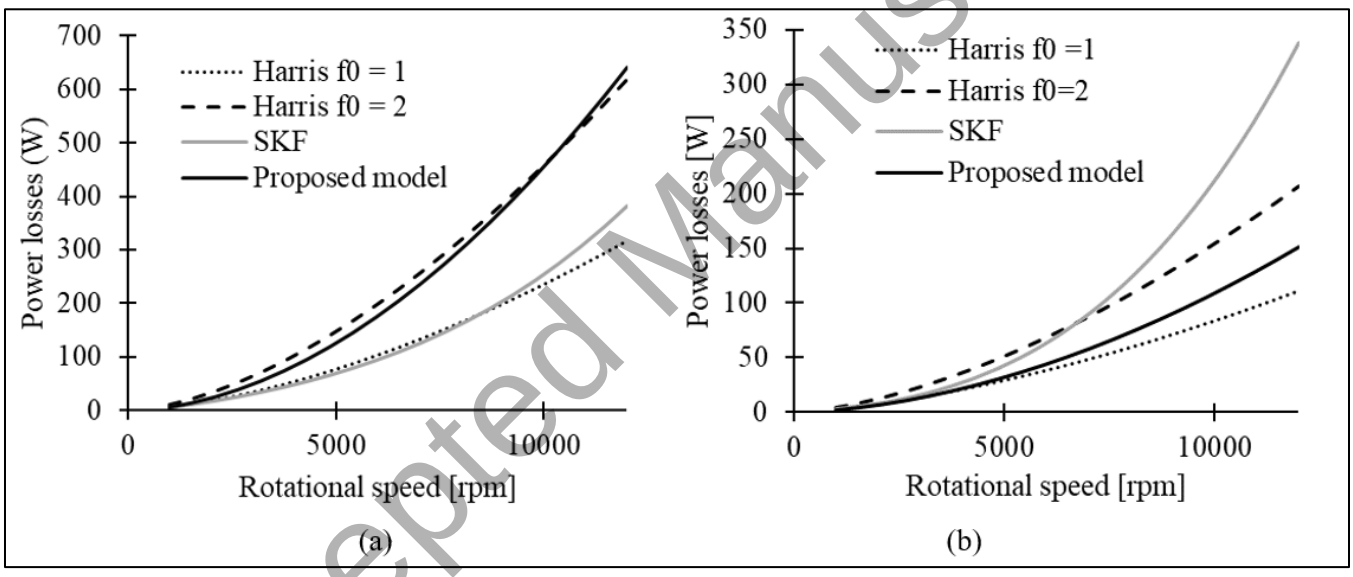

Figure 4 Comparison between SKF, Harris and proposed local model vs rotational speed; (a) Temperature = 30°C; (b) Temperature = 90°C

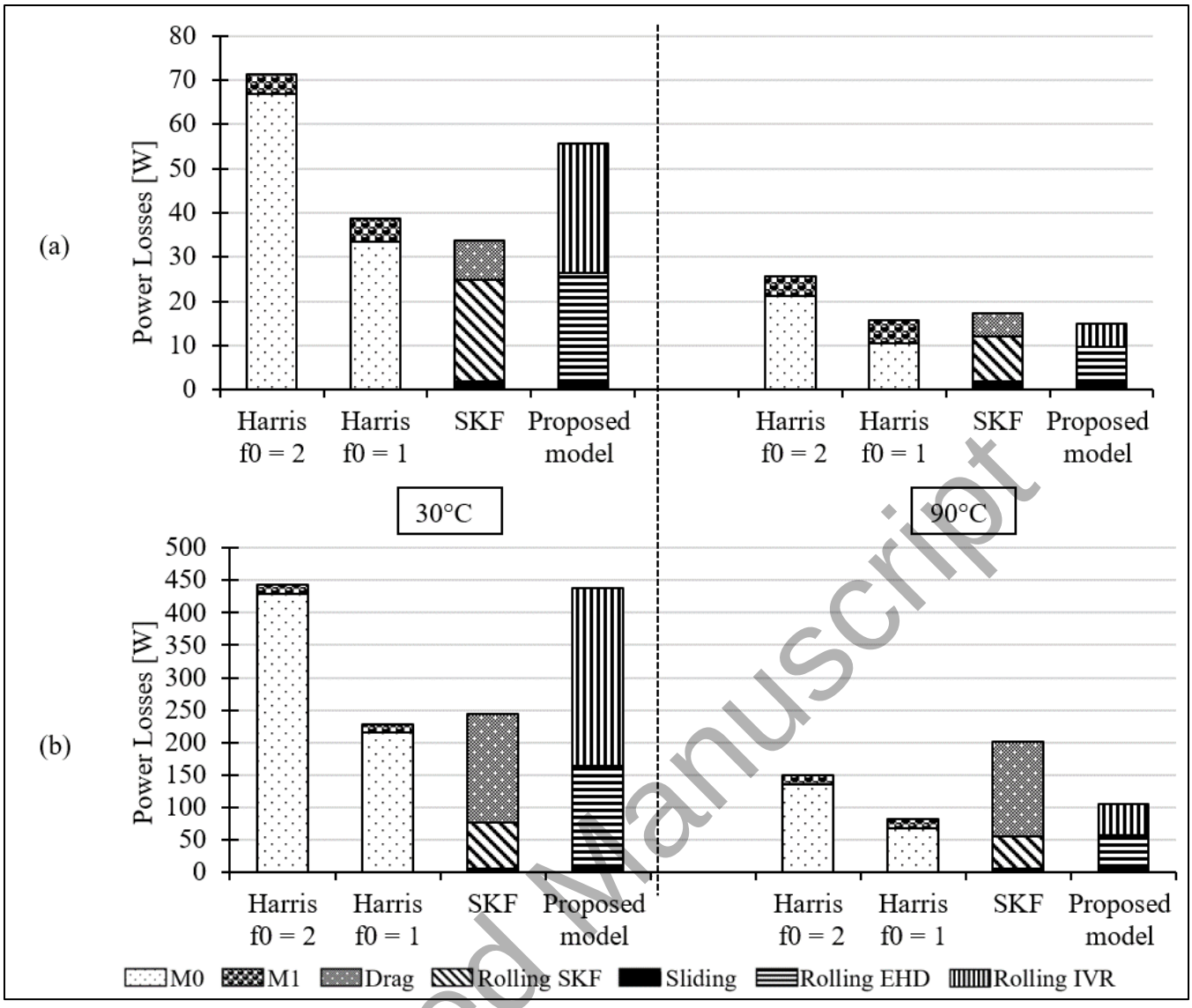

Figure 5 Comparison between SKF, Harris and proposed local model for two different speeds and temperatures. (a) Rotational speed = 3200 rpm; (b) Rotational speed = 9800 rpm.

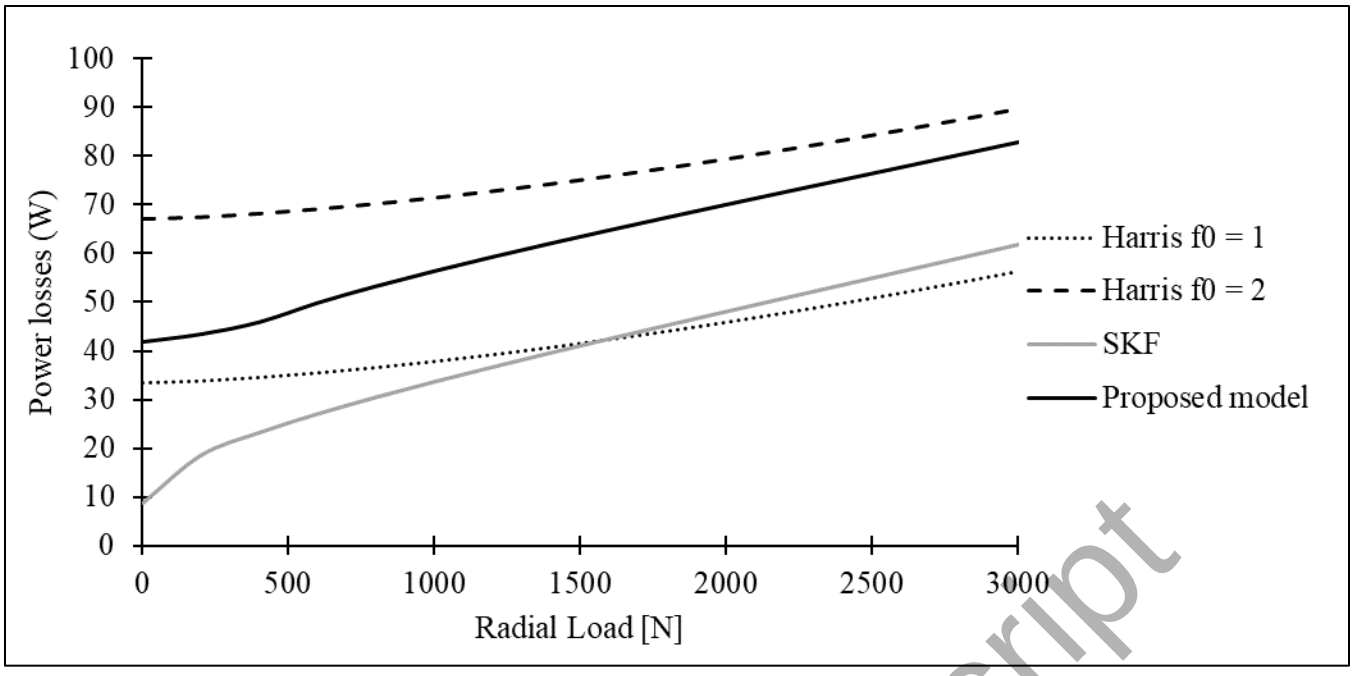

Figure 6 Comparison between SKF, Harris and proposed local model vs applied load. Temperature = 30°C – Speed = 3200rpm.

Table 1 REB characteristics

Mean diameter (mm)	70
Outer diameter (mm)	90
Bore diameter (mm)	50
Contact angle (°)	0
Width (mm)	20
Number of balls (-)	10

Table 2 Oil characteristics

Kinematic viscosity at 40°C (cSt)	36.6
Kinematic viscosity at 100°C (cSt)	7.8
Density at 15°C ($kg.m^{-3}$)	864.6
Pressure-viscosity coefficient (Pa^{-1})	$20 * 10^{-9}$

Table 3 Steel properties

Young's modulus (GPa)	210
Poisson coefficient (-)	0.3